Oct 26th, 12:00 AM

GBT-based Analysis of the Local and Global Buckling of Cold-formed Steel Frames

Cilmar Basaglia

Dinar Camotim

Eighteenth International Specialty Conference on Cold-Formed Steel Structures
Orlando, Florida, U.S.A, October 26 & 27, 2006

GBT-Based Analysis of the Local and Global Buckling Behavior of Cold-Formed Steel Frames

Cilmar Basaglia[1], Dinar Camotim[2] and Nuno Silvestre[3]

Abstract

This paper reports the results of an ongoing investigation on the use of Generalized Beam Theory (GBT) to assess the global and local buckling behavior of cold-formed steel frames. After a brief overview of the main concepts and procedures involved in performing a GBT buckling analysis, one presents the formulation and implementation of a GBT-based beam finite element including global and local deformation modes. Next, one addresses the constraint conditions used to simulate the local displacement compatibility at a frame joint connecting two non-aligned U-section (channel) members. Finally, in order to illustrate the application and capabilities of the proposed GBT finite element formulation, one presents and discusses numerical results concerning the local and global buckling behavior of a simple "L–shaped" frame acted by loadings causing only member compression. For validation purposes, most GBT-based results are compared with values yielded by shell finite element analyses carried out in the code ANSYS.

Introduction

The use of cold-formed steel profiles in the construction industry as been growing steadily in the last few years – this is mostly due their high structural efficiency (large strength-to-weight ratio), remarkable fabrication versatility and

[1]Ph.D. Student, [2]Associate Professor and [3]Assistant Professor, Civil Eng. Dept., IST/ICIST, Technical University of Lisbon, Av. Rovisco Pais, 1049-001 Lisboa, Portugal.

increasingly low production and erection costs. This is particularly true in what concerns industrial (predominantly) and residential building frames. However, because cold-formed steel frames are generally formed by open-section thin-walled columns and beams, which have low torsional stiffness and are highly prone to local and global buckling phenomena (as well as to the interaction between them), the rigorous assessment of their structural behavior constitutes a formidable task – at present, it can only be performed by resorting to shell finite element analysis, an approach that involves a very substantial computational effort (including the interpretation of the results) and is still prohibitive for routine applications (*e.g.*, Masarira 2002, Kim & Kang 2004 and MacPhedran & Grondin 2005). Therefore, this type of steel frames is currently design by means indirect methods, based on the safety checking of their individual members, often adopting the "effective width" concept to take into account the local buckling effects.

In order to make the analysis of cold-formed steel frames computationally simpler and more accessible to the average designer, without sacrificing too much the accuracy of the results obtained, it is indispensable to develop easy-to-use numerical tools based on *beam* finite element analysis. However, before this goal can be achieved, two major difficulties must be overcome: (i) the inclusion of local buckling effects in a beam (one-dimensional) finite element formulation and (ii) the handling of the cross-section rotation, warping and transverse (wall) bending transmission at frame joints connecting non-aligned members. As far as the first aspect is concerned, one very promising approach is the use of beam finite elements based on Generalized Beam Theory (GBT), which was originally formulated by Schardt (1989) and has been substantially developed in the last few years (*e.g.*, Camotim *et al.* 2004, 2006). Nevertheless, because all these developments took place solely for isolated members, an important gap remains to be bridged before a GBT-based approach can be successfully applied to assess the local and global structural response of thin-walled frames.

In the context of the *global* structural behavior of thin-walled frames, a number of investigations have addressed the transmission of the torsion rotation and warping joint transmission. Among them, it is worth mentioning the works due (i) to Morrell (1979) and Morrell *et al*. (1996), who studied the relationship that must exist between the end section torsional rotations of orthogonal U-section members, and (ii) to Sharman (1985), Krenk & Damkilde

(1991) and Tong *et al.* (2005), who investigated the warping transmission between the end sections of arbitrarily oriented U and I-section members connected at joints with different configurations.

As a first step towards developing a GBT-based finite element approach that makes it possible to assess the (elastic) buckling behavior of plane and spatial thin-walled frames, the authors have very recently formulated and numerically implemented a beam finite element methodology that can perform this task when only *global* instability phenomena occur – *i.e.*, it only involves the four GBT rigid-body deformation modes (Basaglia *et al.* 2006). This methodology includes the definition of "joint elements", which translate the GBT modal "language" into a nodal one (more appropriate to handle joints), and was shown to yield virtually exact results – minute differences with respect to the critical load values and buckling mode shapes obtained through shell finite element analyses.

The objective of this work is to present and discuss the results of an ongoing investigation aimed at extending the above GBT approach, so that it can also assess the *local* buckling behavior of the thin-walled frames. Following a very brief overview of the main concepts and procedures involved in performing a GBT buckling analysis, one presents the formulation and numerical implementation of a GBT-based beam finite element that includes global and local deformation modes. Next, in the context of frames built with U-section (channel) members[1], one (i) reviews the most relevant aspects related to the torsion rotation and warping transmission and (ii) addresses the constraint conditions adopted to simulate the compatibility between the end section local (wall transverse bending) displacements of two non-aligned members connected at a frame joint. Finally, the application and capabilities of the proposed GBT approach are illustrated by presenting and discussing numerical results concerning the local and global buckling behavior of a simple "L–shaped" frame acted by loadings causing only member compression. For validation purposes, most GBT-based results are compared with values yielded by shell finite element analyses carried out in the code ANSYS.

[1] Similar results can be readily obtained for frames built with I-section or Z-section members. The major restriction imposed on the member cross-section shape is the fact that it cannot exhibit distortional buckling. The authors are currently working on the removal of such restriction, thus rendering the proposed approach applicable to a wider variety of member cross-section shapes.

GBT Cross-Section Analysis

Consider a thin-walled prismatic member with the arbitrary (*n*-walled) open cross-section shown in figure 1 – also shown are (i) the coordinates *x*, *s* and *z* (along the member length, cross-section mid-line and wall thickness) and (ii) the associated displacement components *u*, *v* and *w*. In order to comply with the classical thin-walled beam theory (Vlasov 1961), the displacement components $u(x,s)$, $v(x,s)$ and $w(x,s)$ must be expressed as

$$u(x,s)=u_k(s)\phi_{k,x}(x) \quad v(x,s)=v_k(s)\phi_k(x) \quad w(x,s)=w_k(s)\phi_k(x) \quad , \quad (1)$$

where (i) $(.)_{,x} \equiv d(.)/dx$, (ii) the summation convention applies to subscript *k*, (iii) $u_k(s)$, $v_k(s)$ and $w_k(s)$ are the functions characterizing deformation mode *k*, yielded by the GBT cross-section analysis and satisfying Vlasov's assumptions of null membrane shear strains and transverse extensions ($\gamma^M_{;xs}=\varepsilon^M_{;ss}=0$), and (iv) $\phi_k(x)$ are mode amplitude functions defined along the member length.

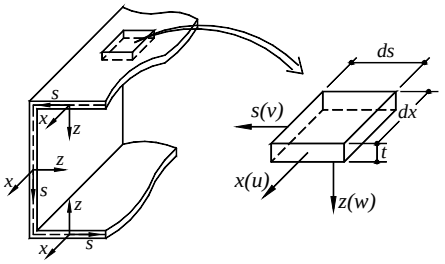

Fig. 1: Arbitrary open cross-section, coordinate axes and displacements

In the context of a GBT cross-section analysis, one considers a discretization into (i) *n+1 natural* nodes (wall ends) and (ii) *m intermediate* nodes, which leads to *n+m+1* deformation modes: (i) the *4* classical rigid-body modes, (ii) *n–3* distortional modes and (iii) *m* local-plate modes (*e.g.*, Camotim *et al.* 2004) – these mode amplitudes are the cross-section degrees of freedom.

To provide some insight on the GBT cross-section analysis procedure and outcome, figures 2(b) and 3 show (i) the discretization adopted to obtain the numerical results presented and discussed ahead in the paper (the member cross-section dimensions and material properties are given in figure 2(a)) and (ii) the in-plane deformed configurations of the *7* (out of *13*) most relevant

deformation modes: axial extension (**1**), major/minor axis bending (**2**, **3**), torsion (**4**), and local-plate (**5** to **7**) modes – recall that an (unlipped) channel cross-section has no distortional deformation modes.

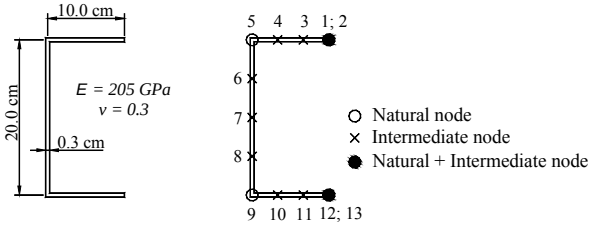

Fig. 2: Cross-section (a) dimensions and (b) GBT discretization

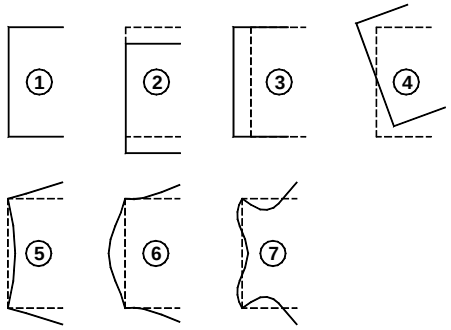

Fig. 3: In-plane shapes of the *7* (out of 13) most relevant deformation modes

GBT Buckling Analysis

The key feature of a GBT analysis resides in the fact that it expresses the cross-section displacement field as a combination of *deformation modes*, which (i) account for both the cross-section in and out-of-plane deformation and (ii) provide an in-depth understanding of the member structural behavior. Once the deformation modes are known, one is able to establish the system of member equilibrium equations

$$C_{ik}\phi_{k,xxxx} - D_{ik}\phi_{k,xx} + B_{ik}\phi_k - \lambda W_j^0 X_{jik}\phi_{k,xx} = 0 \qquad , \quad (2)$$

where (i) λ is the load parameter (ii) X_{jik} are geometric stiffness components associated with the stress resultant $W^{0}_{;j}$ (deemed uniform in this work) and (iii) the components of tensors (matrices) C_{ik}, D_{ik} and B_{ik} are cross-section modal mechanical properties – while C_{ik} and D_{ik} are related to the warping displacements and torsional rotations of the cross-section walls, B_{ik} concerns the cross-section in-plane deformation (distortion and/or transverse bending).

Except for very simple cases, mostly involving simply supported members, system (2) can only be solved by resorting to numerical methods. This fact prompted Silvestre & Camotim (2003) to formulate, implement and validate a GBT-based *beam finite element* intended to perform buckling analyses of thin-walled members – a 2-node beam finite element with $4\times(n+m+1)$ degrees of freedom, based on the mode amplitude function approximation

$$\phi_k(x) = \psi_1(x)Q_{k1} + \psi_2(x)Q_{k2} + \psi_3(x)Q_{k3} + \psi_4(x)Q_{k4} \quad , \quad (3)$$

where (i) $Q_{k1}=\phi_{k,x}(0)$, $Q_{k2}=\phi_k(0)$, $Q_{k3}=\phi_{k,x}(L_e)$ and $Q_{k4}=\phi_k(L_e)$, and (ii) the functions $\psi_i(x)$ are standard Hermite cubic polynomials, defined by ($\xi=x/L_e$, where L_e is the element length)

$$\begin{aligned} \psi_1 &= L_e(\xi^3 - 2\xi^2 + \xi) & \psi_2 &= 2\xi^3 - 3\xi^2 + 1 \\ \psi_3 &= L_e(\xi^3 - \xi^2) & \psi_4 &= 3(\xi^2 - 2\xi^3) \end{aligned} \quad . \quad (4)$$

After introducing (3) into (2) and carrying out the appropriate integrations, one obtains the usual finite element matrix equation

$$([K_e] + \lambda[G_e])\{d_e\} = \{0\} \quad , \quad (5)$$

where $[K_e]$, $[G_e]$ and $\{d_e\}$ are the elementary linear stiffness matrix, geometric stiffness matrix and generalized displacement vector (dimension $4\times(n+m+1)$).

The degrees of freedom associated with each deformation mode, shown in figure 4, are designated as follows: (i) the major/minor axis bending transverse displacements and rotations (modes **2** and **3**) are v_a (d_{22} + d_{32}) and θ_a (d_{21} + d_{31}), for $x=0$, and v_b (d_{24} + d_{34}) and θ_b (d_{23} + d_{33}), for $x=L_e$, (ii) the torsional rotation and its derivative (mode **4** – the latter concerns warping) are φ_a (d_{42}) and φ'_a (d_{41}), for $x=0$, and φ_b (d_{44}) and φ'_b (d_{43}), for $x=L_e$, (iii) the axial displacement and its primitive (mode **1**) are u_a (d_{11}) and $\int u_a$ (d_{12}), for $x=0$, and u_b (d_{13}) and $\int u_b$ (d_{14}), for $x=L_e$, and (iv) the local displacements

and their derivative (modes $k>n+1$) are β_a (d_{k2}) and β'_a (d_{k1}), for $x=0$, and β_b (d_{k4}) and β'_b (d_{k3}), for $x=L_e$ – note that the inclusion the axial displacement primitive among the elementary degrees of freedom makes it possible to "homogenize" system (2), in the sense that it contains only 4th-order differential equations, thus enabling the use of the same Hermite cubic polynomials to approximate all mode amplitude functions – of course, $\phi_1(x)=\int u(x)dx$ has no obvious physical meaning (but one has $\phi_{1,x}(x)=u(x)$).

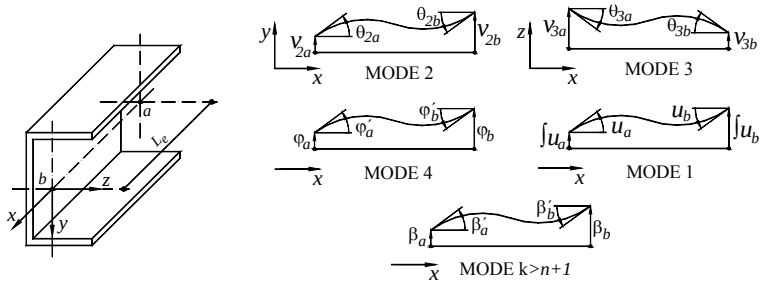

Fig. 4: Degrees of freedom associated each deformation modes

The overall linear and geometric stiffness matrices of a given structural system are obtained by "combining" their elementary counterparts, by means of the well-known "incidence matrix" concept. Although this is a fairly trivial procedure for isolated members (each node is shared by only two equally oriented elements), its extension to frames poses several difficulties. Indeed, the fact that the finite elements (members) connected at a frame joint exhibit different orientations makes it necessary to account for the effects stemming from the need to ensure compatibility between the degrees of freedom of the converging end cross-sections.

Next, one describes the determination of the frame overall total stiffness matrix, on the basis of the associated *GBT-based* elementary matrices:

(i) After discretizing the frame, one must handle separately the member (i_1) internal nodes and (i_2) end nodes associated with frame joints (connecting members with different orientations) – see figures 5(a)-(b). In the internal nodes, the compatibility of the GBT degrees of freedom offers absolutely no difficulties (*e.g.*, Silvestre & Camotim 2003). However, the same does not remain true for the end nodes corresponding to frame joints (*e.g.*, nodes b_r and a_{r+1} in fig. 5(b)), as

these degrees of freedom must be transferred to a "joint element" (see fig. 5(c)). Naturally, all the connection compatibility issues are incorporated into this element, through (i_1) the transformation of the GBT modal degrees of freedom into generalized nodal displacements (reference axes $\bar{x}-\bar{y}-\bar{z}$) of the (idealized) point where the connection is assumed to take place, designated in this work by $O;^{-}$ (see fig. 5(d)) and corresponding to the intersection of the arbitrary reference axes of the various converging members (*e.g.*, axis x in figure 6(a)), and (i_2) the imposition of "*constraint conditions*" that simulate the end section local displacement behavior – these procedures make it possible to quantify the warping and local displacement transmission between the members converging at the joint.

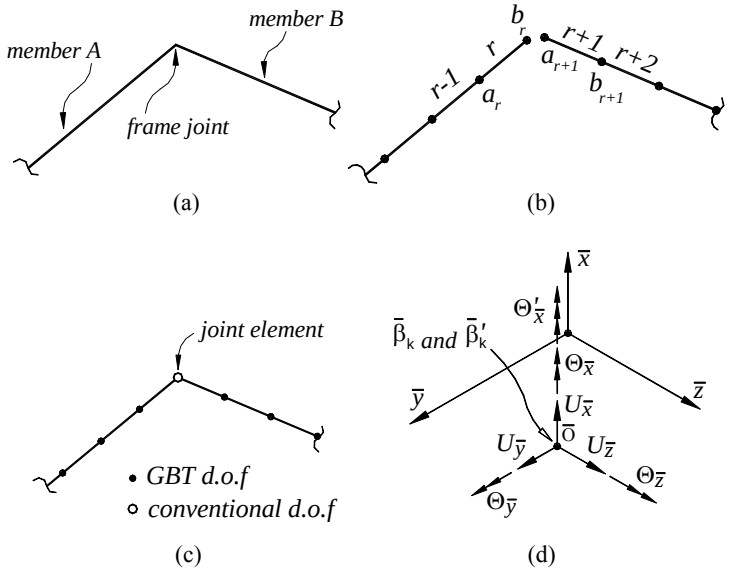

Fig. 5: (a) Frame joint, (b) discretisation of the converging members, (c) "joint element" concept and (d) associated coordinate system

(ii) In order to ensure the displacement compatibility at the "joint element", as illustrated in figures 6(a)-(b), one must use the transformation matrix $[T]$, defined by the expressions

$$\{\bar{\xi}\}=[T]\{d\}=\begin{bmatrix}[R_{\bar{y}+\bar{z}}][R_x][L]_{6x6} & \\ & [I]_{2m+1x2m+1}\end{bmatrix}\{d\} \quad , \quad (6)$$

$$\{\bar{\xi}_i\}=[U_{\bar{x}}\ U_{\bar{y}}\ U_{\bar{z}}\ \Theta_{\bar{x}}\ \Theta_{\bar{y}}\ \Theta_{\bar{z}}\ \Theta'_{\bar{x}}\ \bar{\beta}_{k=n+2}\ \bar{\beta}'_{k=n+2}\ \cdots\ \bar{\beta}_{k=n+m+1}\ \bar{\beta}'_{k=n+m+1}]^T \quad , \quad (7)$$

$$\{d_i\}=[u\ v_y\ v_z\ \varphi_x\ \theta_y\ \theta_z\ \varphi'\ \beta_{k=n+2}\ \beta'_{k=n+2}\ \cdots\ \beta_{k=n+m+1}\ \beta'_{k=n+m+1}]^T$$

where $[R_{\bar{y}+\bar{z}}][R_x][L]$ concerns the rigid-body deformation modes: while (ii$_1$) matrix $[R_{\bar{y}+\bar{z}}]$ describes the transformation associated with two successive rotations, about axes $\bar{y}$ and $\bar{z}$ (see fig. 6(a)), (ii$_2$) matrix $[R_x]$ is related to the transformation related to a rotation about the member axis x (see fig. 6(b)) and (ii$_3$) matrix $[L]$ corresponds to the translation that accounts for the transference of the member generalized displacements from the member centroidal (G) or shear centre (S) longitudinal axis to the reference one passing in $O;^{-}$ (see fig. 6(b)). Moreover, (ii$_1$) $\{\bar{\xi}\}$ is the generalized displacement vector, (ii$_2$) the vector $\{d\}$ components are the GBT degrees of freedom and (ii$_3$) $[I]$ is the identity matrix associated with the local deformation modes and the torsional rotation derivative. The direction cosines appearing in matrices $[R_{\bar{y}+\bar{z}}]$ and $[R_x]$, as well as the components of matrix $[L]$, were recently reported by the authors (Basaglia *et al.* 2006) – due to space limitations, they are not presented here.

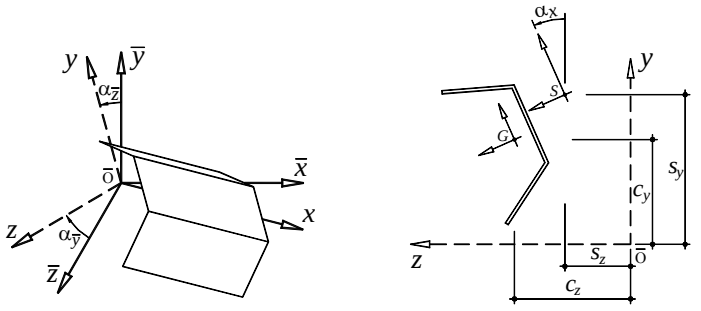

(a) (b)

Fig. 6: (a) Global and member coordinate systems and (b) relative positions of the member cross-section centroid, shear centre and point $O;^{-}$

(iii) By using the transformation matrix defined in (6), one obtains, in each converging member joint end section, *7* degrees of freedom associated with global deformation modes and *2m* degrees freedom associated with local ones. These two sets of degrees of freedom satisfy the conditions

$$\left\{\overline{\xi}\right\}_{b_r} = \begin{bmatrix} [I]_{6x6} & & \\ & \Gamma & \\ & & [I]_{2mx2m} \end{bmatrix} \left\{\overline{\xi}\right\}_{a_{r+1}} \quad , \quad (8)$$

where (iii$_1$) $[I]$ is the identity matrix, (iii$_2$) Γ is a constant relating the torsional rotation derivatives, *i.e.*, that quantifies the "warping transmission" at the frame joint under (a detailed explanation about this concept can be found in Basaglia *et al.* 2006).

(iv) Concerning the local displacement compatibility at the frame joint, one must impose "*constraint conditions*" that (iv$_1$) depend on the joint type and member geometry and (iv$_2$) involve *j* intermediate nodes of the converging member end sections – they are expressed as

$$\Pi_j = \left\{\Delta\right\}^T \left\{\phi_k\right\} = 0 \quad , \quad (9)$$

where the vector $\{\Delta\}$ components are the local mode displacement fields $w_k(s)$ ($k > n+2$). The particular "*constraint conditions*" considered in this work will be addressed in the next section.

(v) Using equations (6), (8) and (9), one readily obtains the frame total stiffness matrix K_T, already ensuring degree of freedom compatibility at all nodes – as far as the rigid-body deformation modes are concerned, K_T is associated with "mixed degrees of freedom": GBT degrees of freedom (d_{ki}) in member internal nodes and "conventional" generalized displacements ($\overline{\xi}_i$) in joint nodes.

Once the frame total stiffness matrix K_T is known, performing its buckling analysis merely consists of solving the standard eigenvalue problem

$$K_T(\lambda) \cdot \delta = 0 \quad , \quad (10)$$

where (i) $\{\delta\}$ is a "mixed" vector combining generalized displacements and GBT degrees of freedom and (ii) λ is the *load parameter* (all applied loads depend linearly on λ). One determines the frame bifurcation loads λ_b

and corresponding buckling mode shapes $\{\delta\}_b$ – the critical ones are λ_{cr} (lowest λ_b) and $\{\delta\}_{cr}$. In order to provide a *modal* representation of the member deformed configurations associated with the frame buckling modes, one must transform the joint nodal generalized displacements (sub-vector $\{\bar{\xi}\}_b$ of $\{\delta\}_b$) back into GBT degrees of freedom concerning the converging member end nodes (sub-vector $\{d\}_b$) – this is done by means of the relation

$$\{d\}_b = [T]^{-1}\{\bar{\xi}\}_b \quad , \quad (11)$$

i.e., by performing an operation which "inverts" the one defined in (6).

Finally, once the values of the GBT degrees of freedom are known in all member nodes, it is a straightforward task to obtain the modal representation of the frame buckling mode, *i.e.*, to identify and quantify the individual contributions of the various member deformation modes.

Constraint Conditions – Joint Connecting Two Channel Members

Consider a frame joint schematically depicted in figure 7(a), connecting two identical non-aligned channel members with their flanges lying in the same planes. Whenever these members experience local deformations, the shell finite element model shown in figure 7(c) provides evidence that, at that joint, (i) the web remains undeformed and (ii) there is full local displacement continuity at the flanges. On the basis of these shell finite element results (and similar ones obtained for joints connecting identical I-section members with the flanges also lying in the same planes), it was possible to conclude that the constraint conditions ensuring local displacement compatibility at this type of joint can be expressed *approximately* by two sets of equations: (i) one imposing the equality between the transverse bending displacements occurring at the points of intersection of the flange free edges (points Q' and Q'' in fig. 7(a)) and (ii) the other imposing null displacements at the intermediate nodes of the member webs[1].

In the particular case of the joint shown in figure 7(a), the first constraint condition set ($\Pi^I_{Q'}$ and $\Pi^I_{Q''}$) involves the flange free end nodes Q'_A, Q'_B, Q''_A and Q''_B, lying on member cross-sections located at a distance f from its

[1] Although shell finite element results were obtained only for channel and I-section member joints, the authors believe that these findings apply also to members with other cross-section shapes.

end – as shown in figures 7(a)-(b), these points correspond to the "idealized" junctions of the members *A* and *B* flange free longitudinal edges. Then, one has

$$\Pi^{I}_{Q'} = \sum_{k=n+2}^{n+m+1} w_k(m_{Q'_A})\phi_k(x_{Q'_A}) - \sum_{k=n+2}^{n+m+1} w_k(m_{Q'_B})\phi_k(m_{Q'_B}) = 0$$
$$\Pi^{I}_{Q''} = \sum_{k=n+2}^{n+m+1} w_k(m_{Q''_A})\phi_k(m_{Q''_A}) - \sum_{k=n+2}^{n+m+1} w_k(m_{Q''_B})\phi_k(m_{Q''_B}) = 0 \quad , \quad (12)$$

where

$$x_{Q'_B} = x_{Q''_B} = f = b \cdot tan(\alpha/2) \qquad x_{Q'_A} = x_{Q''_A} = L_A - f \quad , \quad (13)$$

(i) L_A is the member *A* length (ii) α is the angle between the member axes and (iii) *b* is the horizontal distance from the flange free end to *G* (see fig. 7(b)).

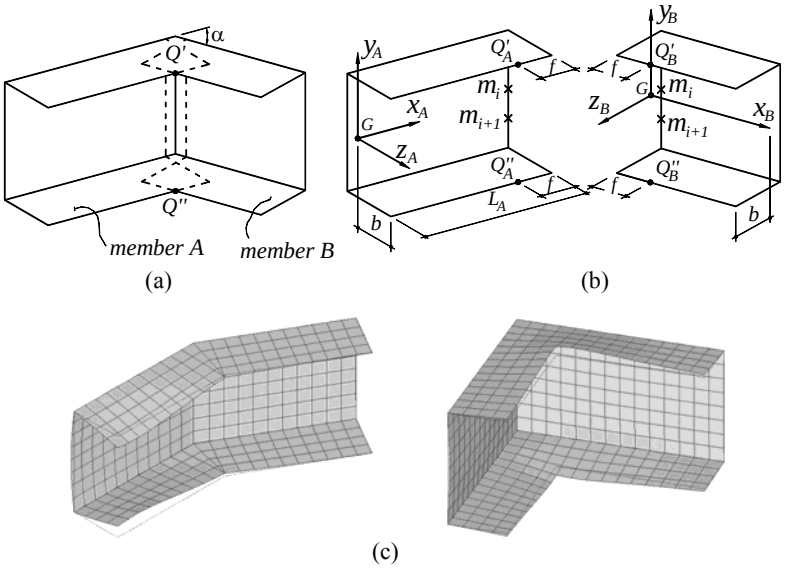

Fig. 7: (a) Joint connecting channel members (flanges in the same planes), (b) illustration of the nodes materializing the joint boundary conditions and (c) shell finite element modeling of the local displacement compatibility

Concerning the second set of constraint conditions Π_i^{II}, it enforces null transverse bending displacements at all the web intermediate nodes of members *A* and *B*[1]. Then, for a web with *i* intermediate nodes one has

$$\Pi_i^{II} = \sum_{k=n+2}^{n+m+1} w_k(m_i)\overline{\beta}_k = 0 \quad . \quad (14)$$

At this stage, it should be mentioned that the well-known *Lagrange multiplier* technique (*e.g.*, Zienkiewicz & Taylor, 2000) provides an alternative (and probably more effective) way to include the above constraint conditions in the frame buckling analysis – it leads to an "enlarged" stiffness matrix with more degrees of freedom. The authors are currently exploring this approach.

Illustrative Examples

In order to validate and illustrate the application and capabilities of the proposed GBT-based beam finite element approach, one now presents and discusses numerical results concerning the local and global elastic spatial buckling behavior of "L–shaped" plane frames of the type shown in figure 8, formed by two orthogonal channel members (members *A* and *B*) having identical cross-sections, connected with flange continuity and subjected to loads causing only member axial compression – while member *A* has a fixed and warping-prevented end section, member *B* is simply supported (warping –free and locally/globally pinned end section). The member cross-section dimensions are the ones given in figure 2(a) and the elastic constant values adopted are $E=205\,GPa$ (Young's modulus) and $\nu=0.3$ (Poisson's ratio). For validation purposes, several GBT-based buckling results are compared with values yielded by finite element analyses performed in the code ANSYS (SAS, 2004) and discretizing the frame into shell element meshes – the particular element adopted is termed SHELL181 (ANSYS nomenclature) and was used with a "full integration" option.

Two different frame geometries (member lengths) were considered, namely (i) $L_A=L_B=70\,cm$ (Case I – two short members) and (ii) $L_A=70cm$ and $L_B=700\,cm$ (Case II – one short and one long member). The member axial compression values are $N_A=P$ and $N_B=\gamma P$ (P is the frame load parameter) –

[1] Note that this procedure *does not* enforce null web transverse bending displacements *exactly*.

one considers $\gamma=1$ in Case I and $\gamma=0.5$ in Case II. Since the members are connected with flange continuity, their end sections exhibit exactly the same warping displacements (they may be viewed as the two "faces" of a single cross-section), which means that the warping transmission is *complete* and *direct – i.e.*, one has $\overline{\varphi}'_A = \overline{\varphi}'_B$ or, equivalently, $\Gamma=1$ must be inserted in (8).

Case I. While (i) figure 9 shows the member *A* and *B* modal amplitude functions associated with the frame critical buckling mode, (ii) figures 10(a)-(b) provide the corresponding deformed configurations obtained by means of (i) a GBT-based finite element analysis (considering *6* elements along the member length, amounting to *59* degrees of freedom) and (ii) the ANSYS shell finite element analysis (mesh associated with more than *5700* degrees of freedom). The comparison between the buckling results yielded by both formulations prompts the following remarks:

(i) First of all, the critical loads obtained through the two analyses virtually coincide: $P_{cr.GBT}=150.09kN$ and $P_{cr.ANSYS}=150.44kN$ – *0.25%* error).

(ii) The buckling mode shapes shown in figures 10(a)-(b) are remarkably similar. Moreover, the detail of the GBT one depicted in figure 10(c) provides insight on how the flange transverse bending displacement continuity was modeled in the GBT approach: one just imposes it on the two common flange free edge points – however, note that it reproduces quite accurately the deformed shape yielded by the ANSYS analysis.

(iii) The frame buckles in a local mode that (iii_1) involves the two members and (iii_2) includes participations of the GBT deformation modes **5** and **6**.

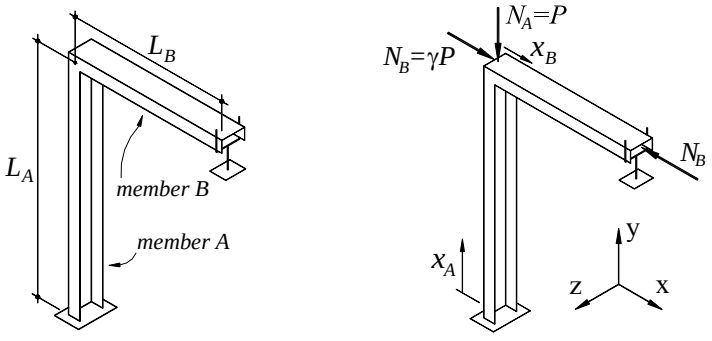

Fig. 8: "L– shaped" frame geometry, loading and end support conditions

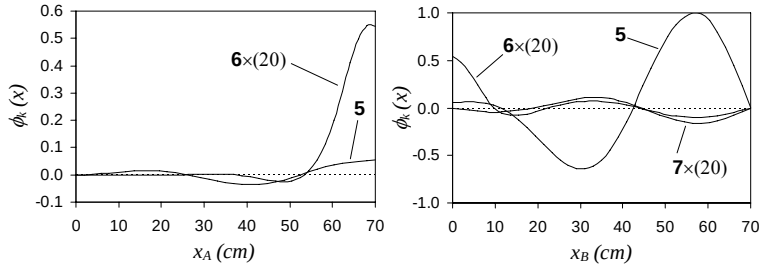

Fig. 9: Member modal amplitude functions $\phi_k(x)$ – Case I

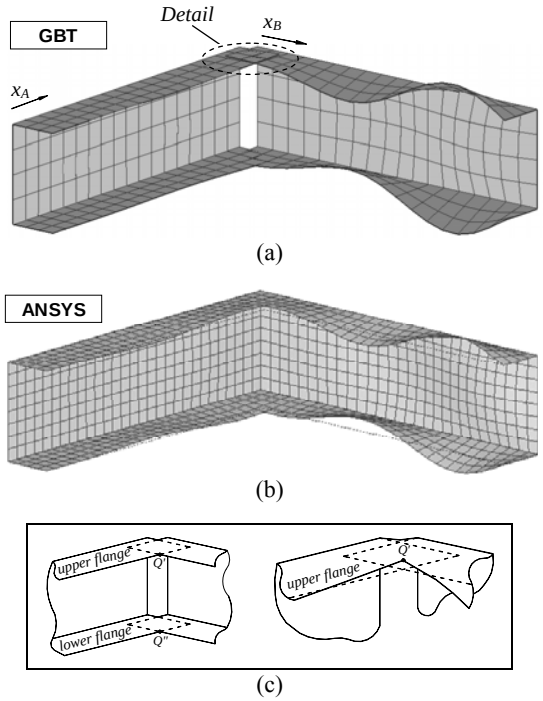

Fig. 10: Critical buckling mode shapes yielded by the (a) GBT and (b) ANSYS analyses (Case I); (c) detail of the GBT modeling of the frame joint

(iv) Obviously, the participation of the local modes is more meaningful in the (simply supported) member *B*. Moreover, this participation is higher between mid-span and the simple support.

(v) The participation of mode **6** reaches a maximum in the vicinity of the joint and becomes null at the member *A* mid-span. Moreover, there is no transmission of mode **7** across the joint – it only appears in member *B*.

Case II. Figures 11(a)-(c) show the member *A* and *B* modal amplitude functions concerning the frame three first buckling modes. Figures 12(a)-(c), on the other hand, provide the corresponding buckling mode shapes obtained by means of ANSYS analyses – in the second and third modes, only the member *A* deformed configuration is displayed. While the GBT analysis was based on a frame discretization into *16* elements (*9* in member A and *7* in member *B* – *216* degrees of freedom), the ANSYS analysis involved more than *17000* degrees of freedom. After comparing the buckling results yielded by the two analyses, one is led to the following conclusions:

(i) Once again, there is a very good correlation between the two buckling load sets: (i_1) $P_{cr.GBT}$*=153.27kN* and $P_{cr.ANSYS}$*=153.79kN* (*0.34%* error) (i_2) $P_{b2.GBT}$*=160.29kN* and $P_{b2.ANSYS}$*=160.58kN* (*0.18%* error) and (i_3) P_{GBT}*=167.82kN*, P_{ANSYS}*=164.27kN* (*2.2%* error).

(ii) There is also a rather close agreement between the buckling mode shapes shown in figures 12(a)-(c) and the modal amplitude functions displayed in figures 11(a)-(c). However, the latter are considerably richer, in the sense that provide a much deeper insight on both the frame mechanical behavior and how the joint influences it.

(iii) The virtual coincidence of the frame buckling loads and mode shapes is even more remarkable and striking if one thinks that the numbers of degrees of freedom required to perform similarly accurate GBT and ANSYS analyses are very far apart (their ratio is about *80*).

(iv) The frame critical buckling occurs in a lateral-torsional mode (combination of deformation modes **2** and **4**) which obviously involves mostly the longer member *B* – note that the contribution of mode **2** reaches its highest value at mid-span.

(v) Concerning the second buckling mode, it involves the occurrence of local deformations in member *A* – *2* half-waves with a predominant contribution from mode **5**. As for the third buckling mode, it basically involves the participation of (v_1) local modes in member *A* (mostly

mode **5**, with 3 half-waves, but also modes **6** and **7**) and (v_2) mode **3** (minor axis bending with a single half-wave) in member *B*.

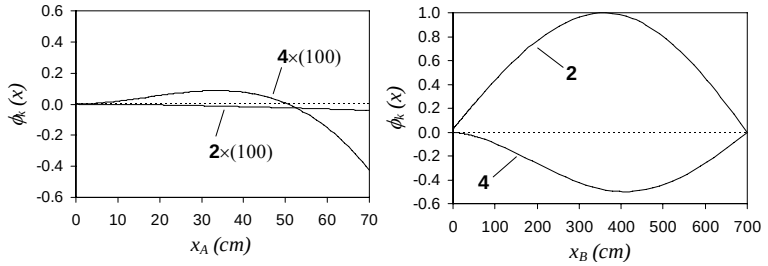

(a)

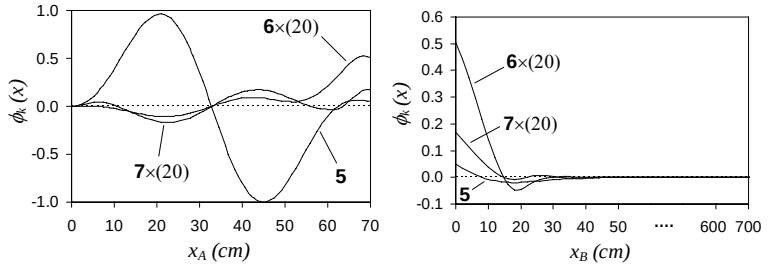

(b)

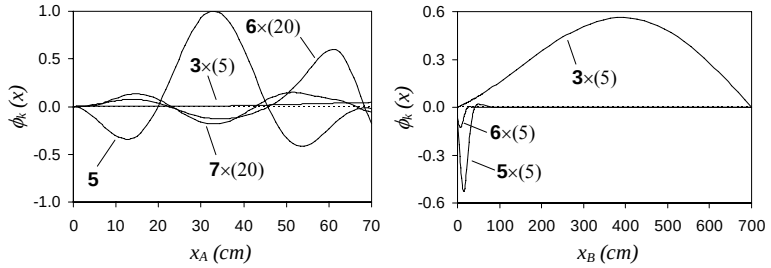

(c)

Fig. 11: Member modal amplitude functions $\phi_k(x)$ for the (a) critical, (b) second and (c) third buckling modes – Case II

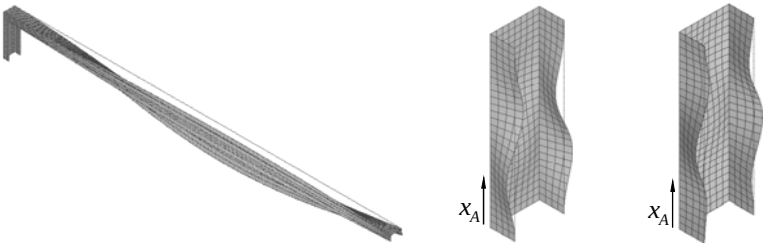

(a) (b) (c)

Fig. 12: (a) Critical, (b) second and (c) third buckling mode shapes yielded by the ANSYS analysis (Case II) – only member *A* in the latter two

(vi) Figures 11(b)-(c) clearly reveal the effects of the compatibility of the local displacements at the frame joint – note that, in member *B*, local modes only appear in the close vicinity of the frame joint.

Conclusion

This paper presented the mains steps and procedures involved in the formulation and numerical implementation of a GBT-based beam finite element intended to analyze the global and local buckling behavior of cold-formed steel frames. After a very brief review of the most relevant concepts involved in the performance of a GBT-based buckling analysis, the paper addressed in detail (i) the formulation of a GBT-based beam finite element and (ii) its use to determine the frame linear and geometric stiffness matrices. Next, one developed constraint conditions making it possible to model the local displacement compatibility at the end sections of two non-aligned channel members connected at a frame joint (with flange continuity). Finally, in order to illustrate the application and capabilities of the proposed GBT-based beam finite element formulation, numerical results concerning the global and local buckling behavior of simple "L-shaped" frames were presented and discussed – for validation purposes, some of these results were also compared with values yielded by shell finite element analyses performed in the code ANSYS. The GBT approach was found (i) to exhibit a high numerical efficiency (one consistently obtained virtually exact results with a very small number of degrees of freedom – considerably smaller that the one required to perform equally accurate ANSYS analyses) and (ii) to provide deep insight on the mechanics of the frame buckling behavior.

Acknowledgements

The first author gratefully acknowledges the financial support of Programme Alβan (European Union Programme of High Level Scholarships for Latin America), through scholarship nº E04D029316BR.

References

Basaglia C., Camotim D. and Silvestre N. (2006). Formulation of a GBT-based finite element to analyse the global buckling behaviour of plane and spatial thin-walled frames, *Proceedings of III European Conference on Computational Mechanics: Solids, Structures and Coupled Problems in Engineering* (ECCM 2006 – Lisboa, 5-9/6). (in press)

Camotim D., Silvestre N., Gonçalves R. and Dinis P.B. (2004). GBT analysis of thin-walled members: new formulations and applications. *Thin-Walled Structures: Recent Advances and Future Trends in Thin-Walled Structures Technology* (International Workshop – Loughborough, 25/6), J. Loughlan (ed.), Canopus Publishing Ltd., Bath, 137-168.

Camotim D., Silvestre N., Gonçalves R. and Dinis P.B. (2006). GBT-based structural analysis of thin-walled members: overview, recent progress and future developments, *Advances in Engineering Structures, Mechanics and Construction* (SMCD –Waterloo, 14-17/5), M. Pandey, W. Xie and L. Xu (eds.), Springer Science, Dorderecht. (in press)

Kim S.E. and Kang K.W. (2004). Large-scale testing of 3-D steel frame accounting for local buckling, *International Journal of Solids and Structures*, **41**(18-19), 5003-5022.

Krenk S. and Damkilde L. (1991). Warping of joints in I-beam assemblages. *Journal of Engineering Mechanics* (ASCE), **117**(11), 2457-2474.

Masarira A. (2002). The effect of joints on the stability behaviour of steel frame beams, *Journal of Constructional Steel Research*, **58**(10), 1375-1390.

MacPhedran I. and Grondin G. (2005). Warping restraint and steel frame instability, *Proceedings of SSRC Annual Stability Conference* (Montreal – 6-9/4), 205-224.

Morrell P. (1979). The influence of joint detail on the torsional behaviour of thin-walled structures having an axial discontinuity, *Thin-Walled Structures* (Strathclyde – 3/6/4), Granada, London, 539-552.

Morrell P., Riddington J., Ali F. and Hamid H. (1996). Influence of joint detail on the flexural-torsional interaction of thin-walled structures. *Thin-Walled Structures*, **24**(2), 97-111.

Schardt R. (1989). *Verallgemeinerte Technishe Biegetheorie*. Springer-Verlag, Berlin. (German)

Sharman P.W. (1985). Analysis of structural with thin-walled open section, *International Journal of Mechanical Sciences*, **27**(10), 665-677.

Silvestre N. and Camotim D. (2003). GBT buckling analysis of pultruded FRP lipped channel members, *Computers & Structures*, **81**(18-19), 1889-1904.

Swanson Analysis Systems Inc. (2004). *ANSYS Reference Manual* (version 8.1).

Tong G., Yan X. and Zhang L. (2005). Warping and bimoment transmission through diagonally stiffened beam-to-column joints, *Journal of Constructional Steel Research*, **61**(6), 749-763.

Vlasov B.Z. (1958). *Thin-Walled Elastic Bars*. Fizmatgiz, Moscow. (Russian – English translation: Israel Program for Scientific Translation, Jerusalem, 1961)

Zienkiewicz O.C. and Taylor R.L. (2000). The Finite Element Method (5^{th} edition), Butterworth-Heinemann, Oxford.